# Low-energy phonon dispersion in $LaFe_4Sb_{12}$

Michael Marek Koza,[1] Martin Boehm,[1] Erik Sischka,[2] Walter Schnelle,[2] Hannu Mutka,[1] and Andreas Leithe-Jasper[2]
[1]*Institut Laue Langevin, 6 Rue Jules Horowitz, B.P. 156, 38042 Grenoble, Cedex 9, France*
[2]*Max-Planck-Institut für Chemische Physik fester Stoffe, Nöthnitzer Straße 40, 01187 Dresden, Germany*
(Received 11 November 2014; published 16 January 2015)

We studied the vibrational dynamics of a single crystal of $LaFe_4Sb_{12}$ by three-axis inelastic neutron spectroscopy. The dispersion of phonons with wave vectors **q** along $[xx0]$ and $[xxx]$ directions in the energy range of eigenmodes with high amplitudes of lanthanum vibrations, i.e., at $\hbar\omega \lesssim 12$ meV is identified. Symmetry-avoided anticrossing dispersion of phonons is established in both monitored directions and distinct eigenstates at high-symmetry points and at the Brillouin-zone center are discriminated. The experimentally derived phonon dispersion and intensities are compared with and backed up by *ab initio* lattice dynamics calculations. Results of the computer model match well with the experimental data.

DOI: 10.1103/PhysRevB.91.014305 PACS number(s): 63.20.−e, 63.20.dd, 25.40.Fq

## I. INTRODUCTION

It has been demonstrated by experiments that the lattice thermal conductivity $\kappa_l$ of the binary skutterudite $CoSb_3$ (space group $Im\bar{3}$) can be strongly suppressed when alloyed with electropositive elements $M$ such as lanthanum and cerium [1–4]. The gradual filling of the large voids in the $CoSb_3$ structure with La and Ce requires an electronic compensation to be accomplished by substituting Co with Fe resulting in the nominal stoichiometry $M_{1-x}Fe_yCo_{4-y}Sb_{12}$. One puzzling outcome of the measurements is the observation that even in the case of a presumably complete filling, i.e., in the ordered structure of the ternary skutterudite $CeFe_4Sb_{12}$ with $x = 0$ and $y = 4$, its $\kappa_l$ remains lowered by more than one order of magnitude compared to $\kappa_l$ of the ordered $CoSb_3$ [4]. Other thermal transport experiments on a series of $MFe_4Sb_{12}$ with $M$ = Ca, Sr, Ba, La, Ce, Pr, Nd, Eu, and Yb support these results [5]. They disclosed a dependence of the effect on the cation properties and extended the temperature scale beyond room conditions.

As lattice thermal transport is accomplished by dispersive phonons it is obvious that the microscopic mechanism responsible for the strong reduction of $\kappa_l$ is to be sought within the interaction between the vibrational dynamics of the electropositive $M$ with acoustic phonons of the anionic $Fe_4Sb_{12}$ matrix. In a recent modeling study Bernstein *et al.* have demonstrated that $\kappa_l$ is highly sensitive to the details of this interaction on the level of the Grüneisen parameters of La-dominated eigenmodes in $LaFe_4Sb_{12}$ [6]. On the grounds of a phenomenological model Geng *et al.* concluded in Ref. [7] that anharmonicity introduced with $M$ = Ca, Ba, and Yb into $Co_4Sb_{12}$- and $Fe_4Sb_{12}$-based skutterudites satisfies to account for the reduction in $\kappa_l$ within a classical scenario of phonon umklapp-scattering processes. The results are thus in coherence with the data of Bernstein and coworkers. The experimental establishment of the anharmonic effects and the deciphering of their details is however elaborate for many reasons connected to the properties of the skutterudite compounds.

The coupling of La and Ce with $Fe_4Sb_{12}$ provokes the formation of vibrational modes with high amplitudes of $M$ at relatively low energies in the range of 5–10 meV [8–12]. Thence, high-energy resolution spectroscopy is required to discriminate distinct phonons at these low energies. Vibrational eigenstates at the Brillouin-zone center (Γ-point excitations) in this energy range are infrared (IR) active. Due to the high reflectivity of the semiconducting and metallic compounds IR spectroscopy proved to be highly challenging and only few reports on the hybrid modes have been published [13,14]. Raman spectroscopy was successfully performed on $La_xFe_3CoSb_{12}$ monitoring however higher energies [15,16].

Another complication stems from the underlying phase diagram of the cobalt- and iron-antimonides making crystal formation difficult. Available single crystals are of a size rather suitable for inelastic x-ray scattering (IXS) experiments with a resolution of ≈1.5 meV, at best. Some information on eigenmodes of $CoSb_3$ could be harvested by the exploitation of the phonon selection rules within the four-dimensional wave vector **Q** and energy $\hbar\omega$ phase space [17]. High-resolution inelastic neutron scattering (INS) on powder material of $LaFe_4Sb_{12}$ was able to discriminate between Γ-point and Brillouin-zone boundary excitations and, thus, between van Hove singularities of acoustic and optic modes in the energy range of 5–10 meV [12]. As a drawback, the orientationally averaged signal monitored the inelastic response dependent on the modulus of the wave vector $|\mathbf{Q}|$ only and did not allow to identify distinct phonon eigenvectors.

Against the aforementioned experimental limitations the results were of high virtue to establish and improve models of the microscopic dynamics by density functional theory (DFT) and lattice dynamics calculations (LDC) [9,12,15,17,18]. Thereby the experimentally established excessive low-energy modes in $LaFe_4Sb_{12}$ were assigned to phonons with enhanced amplitudes of La, of lowered dispersivity, and slightly augmented mode Grüneisen parameters [6,19,20]. The soundness of these findings was scrutinized by IXS and INS experiments on homologous compounds such as $IrSb_3$ and $ROs_4Sb_{12}$ with $R$ = La, Sm in Refs. [21,22], $CeOs_4Sb_{12}$ in Ref. [23], $SmRu_4Sb_{12}$ in Ref. [22], and $CeRu_4Sb_{12}$ in Ref. [24].

Despite the so far conclusive results the understanding of the thermal transport on microscopic levels and the verification of modeling data misses the experimental establishment of three fundamental properties in the phonon dynamics of $LaFe_4Sb_{12}$. First, the direct experimental observation of the low-energy phonon-eigenvector scheme is missing. Second, the anharmonicity of the phonon modes in terms of Grüneisen parameters have not been established yet. Finally, the phonon

 

life times observable as the width of the vibrational eigenstates require an experimental characterization.

This paper presents our next effort to provide this essential information on the dynamics of the ternary skutterudite $LaFe_4Sb_{12}$ in the energy regime of high La amplitudes. We report phonon dispersions along $[xx0]$ and $[xxx]$ directions as probed at room temperature by neutron three-axis spectroscopy on a single-crystal specimen with a volume of $5 \times 5 \times 2\,mm^3$. All acoustic and low-energy optic eigenmodes were discriminated; Γ-point excitations and eigenstates at high symmetry points of the Brillouin-zone boundary were identified. The measurements were accompanied and guided by lattice dynamics calculations whose predictions proved to be of high precision. The phonon dispersion and eigenvectors, i.e., energies and intensities of the probed eigenstates, were characterized satisfactorily.

## II. EXPERIMENTAL PROCEDURE

### A. Synthesis and crystal growth of $LaFe_4Sb_{12}$

Polycrystalline samples of $LaFe_4Sb_{12}$ were synthesized by powder metallurgical techniques. In a first step compacted blends of powders of precursors $FeSb_2$, $LaSb_2$, and Sb (99.99%, Chem Pur) were annealed at 600 °C for one week in glassy carbon crucibles, which were sealed in Ta tubes.

In a typical crystal growth experiment about 4 g of $LaFe_4Sb_{12}$, 0.8 g $LaSb_2$, and 35 g Sb were mixed and compacted. The tablets were placed into a glassy carbon crucible (inner diameter, 20 mm; height, 30 mm) with a lid. This assembly was sealed into a crucible manufactured from Inconel. All these steps were carried out in an argon-gas glove box system (oxygen, and moisture content less than 1 part per $10^6$). The closed Inconel crucible was placed into an electric box-type furnace and subjected to the following heat treatment: (i) initial heating to 650 °C within 24 hours; (ii) additional heating to 830 °C within two hours with a dwell time at this temperature of two hours; (iii) slow cooling to 685 °C within 144 hours followed by a heat treatment at this temperature for 168 hours; (iv) final cooling to 50 °C within 24 hours.

The excess of antimony was removed by sublimation of Sb at 600 °C applying a dynamic vacuum of about $10^{-4}$ mbar. The composition of the grown crystals was investigated by microprobe analysis applying energy dispersive or wave length dispersive spectroscopy, respectively. It was found that their composition tend to vary in the range of $La_{0.90\pm0.04}Fe_4Sb_{12}$. The specimen utilized for this study was handpicked for its large size and its clean morphology. For simplicity we refer to this specimen as $LaFe_4Sb_{12}$ throughout this paper.

### B. Instruments and experimental protocol

Four different neutron-scattering instruments were utilized for the characterization, orientation, and spectroscopic measurements of the single crystalline $LaFe_4Sb_{12}$ specimen. All instruments are located at the European neutron source Institut Laue Langevin (ILL) in Grenoble, France.

The neutron Laue camera OrientExpress@ILL was exploited for the preorientation of the sample. Figure 1 reports two examples of recorded Laue diffractograms. The different orientations of the crystal are indicated by few indexed reflections.

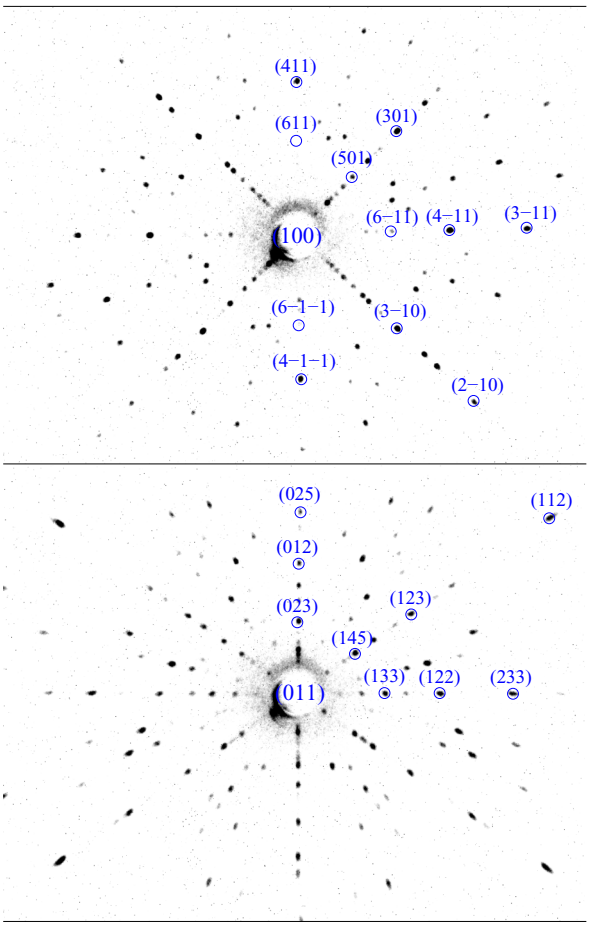


FIG. 1. (Color online) Neutron Laue diffractograms of the $LaFe_4Sb_{12}$ single-crystal sample monitored in two directions. Some reflexes are indexed for demonstration purposes.

A general overview of the dispersion properties and scattering intensities of the acoustic phonons was collected at the single-crystal time-of-flight spectrometer IN5@ILL. The preparatory work was completed at the thermal three-axis spectrometer (TAS) IN3@ILL at which the sample was fine oriented and specific **Q** points and orientations were examined for best scattering intensities. This preparatory work is set aside in this paper. However, it is important to note that the diffractograms recorded at OrientExpress@ILL showed only reflections that could be indexed according to the symmetry and structural properties of the ternary skutterudite compound. In agreement with these results the elastic and inelastic signals observed at IN5@ILL and IN3@ILL gave strong indication of a purely single-crystal nature of the $LaFe_4Sb_{12}$ specimen.

Data reported in this paper were taken at the high-flux thermal TAS IN8@ILL. A Cu(200) monochromator and Cu(200) analyzer configuration were utilized. All phonon scans were carried out with constant $k_f = 2.662\,Å^{-1}$. The majority of scans was performed with an uncollimated beam. A collimation of 60′ was chosen for a few scans of dispersive modes at lowest energies. Elastic scans were performed at some different **Q** points.

The established energy resolution at the elastic $E_0 = 0$ meV position was generally between 0.5 and 0.6 meV, in good

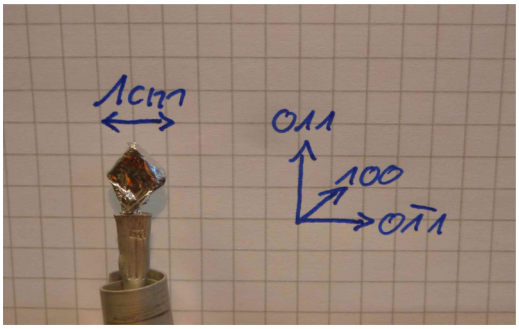


FIG. 2. (Color online) Single-crystal $LaFe_4Sb_{12}$ specimen supported in thin aluminum foil and mounted on the goniometer shielded with cadmium. Indicated are the size and orientation of the crystal matching the top Laue pattern in Fig. 1.

agreement with calculated resolution widths obtained by the TAS simulation package RESTRAX [25].

For sufficient statistical accuracy acquisition was carried out for 250 000 incident monitor counts resulting in an acquisition period of one up to two minutes per single data point with the uncollimated beam and up to five minutes per data point with the collimated beam. Note that for clarity reasons some of the spectra presented in this paper are based on grouped data points and all spectra are scaled as for 25 000 incident monitor counts.

The sample was supported within a thin aluminum foil on a goniometer mounted in an aluminum vacuum chamber with a diameter of 100 cm. Aside from the entrance and exit windows for the neutron beam the entire goniometer, its support, and the vacuum chamber were covered with neutron absorbing cadmium for optimum sample signal to background ratio. Figure 2 shows the sample goniometer setup. Size and orientation of the single crystal are indicated. All measurements were carried out at room temperature and high vacuum. A lattice parameter of $a = 9.135$ Å was determined experimentally.

Two orientations of the specimen were exploited to follow the dispersion of acoustic phonons with $\mathbf{q}||[xx0]$ ($\Gamma$ to $N$) and $\mathbf{q}||[xxx]$ ($\Gamma$ to $P$) directions and to discriminate between different phonon polarizations. Thence, we focused on directions allowing an orientation of the sample face perpendicular to the scattering plane. Scans in the $(x00,0xx)$ plane allowed to monitor the eigenmodes in $[xxx]$ and the transverse acoustic mode of lowest energy in $[xx0]$ direction. Scans in the $(x00,0x0)$ plane completed the eigenmode scheme by the modes of higher energy transverse and longitudinal polarizations in $[xx0]$ direction. Thereby most of the scans were constant $\mathbf{Q}$ runs, a few were carried out at constant energy $\hbar\omega$. Note that $\mathbf{Q} = \mathbf{G}_{hkl} \pm \mathbf{q}$ with $\mathbf{G}_{hkl}$ the reciprocal lattice vector and $\mathbf{q}$ the phonon wave vector is given in relative length units in this paper.

Specific $\mathbf{Q}$ points were chosen according to phonon intensities computed from lattice dynamics calculations (LDC). The LDC were derived from Hellmann-Feynman forces by the direct method implemented in the software package PHONON [26,27]. The Hellmann-Feynman forces were computed through density functional theory (DFT) methods carried out with the Vienna *ab initio* simulation package (VASP) [28,29]. The original calculations were outlined in Ref. [12]. In this paper, however, they have been adapted to the computation approach followed in Ref. [30] having employed a super cell comprising $2 \times 2 \times 2$ unit cells and a $k$-point mesh of $7 \times 7 \times 7$. It is worth noting that we utilized the generalized gradient approximation (GGA) formulated by the Perdew-Burks-Enzerhof (PBE) density functional. This is at variance with the computation study by Feldman *et al.* presented recently in Ref. [20] utilizing the local density approximation (LDA).

Furthermore, we have refined the pristine LDC by taking into account not only DFT Hellmann-Feynman forces but also a few eigenenergies identified at the Brillouin-zone center and specific zone boundary points in the INS spectra. This way a closer match of the primary ground-state dispersion relation with the room temperature experimental data was achieved. Whenever the refined LDC results are employed we refer to them as LDC*.

## III. RESULTS AND DISCUSSION

### A. Phonon spectra and dispersion relation

Figures 3 and 4 report scans $\mathbf{q}||[xx0]$ discriminating the three different polarizations of acoustic phonons. The specific reciprocal space points $\mathbf{Q}$ are indicated in the figures. All spectra are approximated by Gaussian lines and a flat constant background. The number of phonon peaks is chosen according to the LDC results. They are represented by the filled Gaussians in the figures.

To highlight the experimental energy resolution an elastic line scan is indicated in Fig. 3 with the data at $(6, -.1, -.1)$. Remaining unfilled peaks indicate parasitic phonon intensities. As the monochromatic beam was focused vertically, the out-of-plane resolution was coarse (around 0.35 full width at half maximum in reciprocal lattice units as computed with RESTRAX) leading to a crossing of transversal phonon branches along the out-of-plane $[0\bar{x}x]$ direction.

Figure 5 summarizes all phonon energies identified through the LDC-guided fits of Gaussian lines to different scans along $[xx0]$. Note that the low-energy acoustic phonon of transverse polarization (ta1) was scanned along different directions and at different conditions such as with distinct collimations. This strategy was applied to trace as well other modes in particular excitations at high-symmetry points. Thence, the energies reported for the $\Gamma$ point correspond to average values derived from excitations at distinct Brillouin-zone centers.

Dashed lines represent elastic moduli derived from ultrasonic attenuation experiments on a single crystal specimen in equivalent directions [31]. The slope corresponds to values approximated at 140 K, however, the estimated variation of the moduli up to room temperature has a negligible effect on the results sketched in Fig. 5.

Apart from the $\Gamma$-point excitation at $\hbar\omega = 6.72 \pm 0.01$meV, which can be uniquely assigned to a threefold degenerate, infrared-active eigenstate [3Tu(I)] the density of $\Gamma$-point excitations at higher energies is too high to unequivocally discriminate between different eigenfrequencies in this experiment. Although scans at different Brillouin-zone centers resulted in a variation of peak positions and intensities, for example in the energy range of 11–11.5 meV, we do not

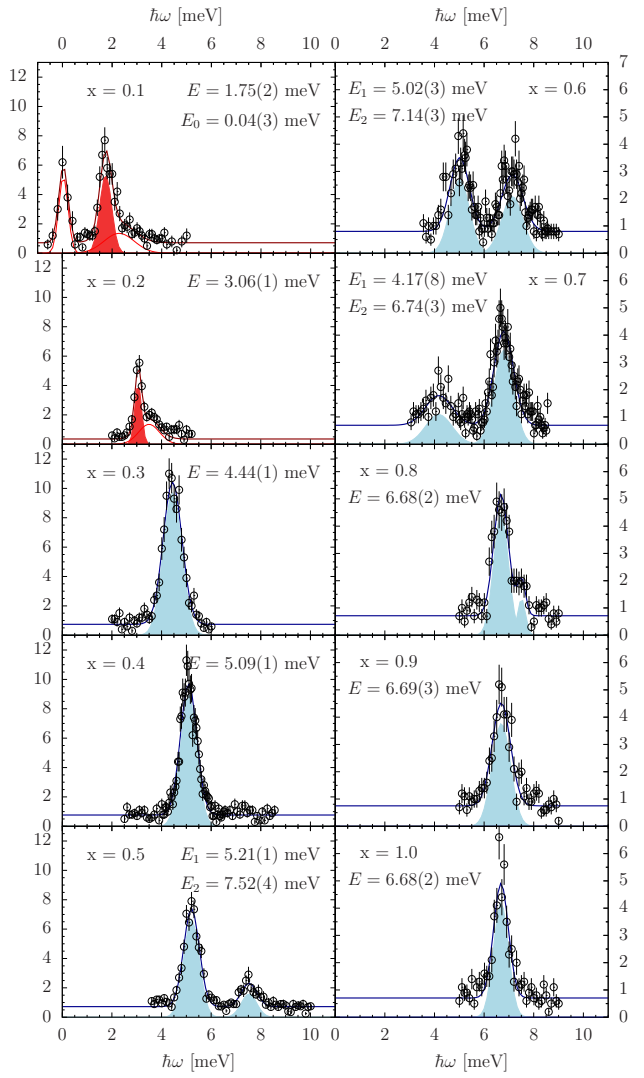


FIG. 3. (Color online) Phonon spectra measured along $[xx0]$ corresponding to $(6,-x,-x)$ scans in reciprocal space. Energies of excitations and $x$ points are indicated in the figures. Intensity corresponds to detector counts per 25 000 counts in monitor. Filled Gaussians represent fit results to the phonon peaks. Total fits are represented by full lines. Red color indicates results with a 60′ collimated beam, blue color represents data with the uncollimated beam.

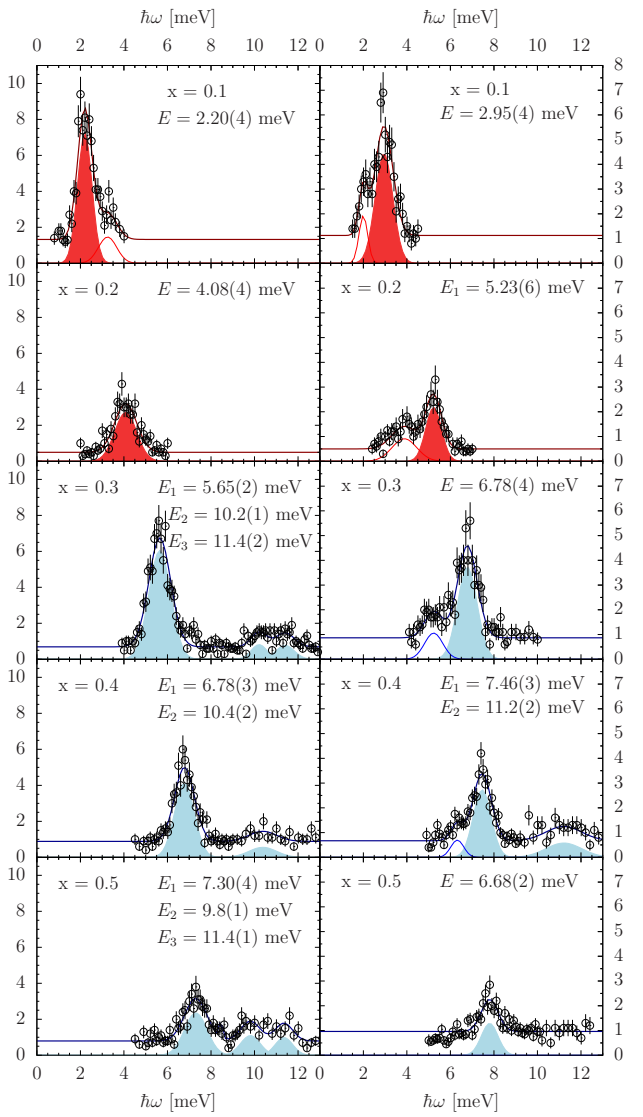


FIG. 4. (Color online) Phonon spectra measured along $[xx0]$ corresponding to scans at $(-5+x,3+x,0)$ and $(-5+x,-3+x,0)$ plotted in the left and right panels, respectively. Energies of excitations and $x$ points are indicated in the figures. Intensity corresponds to detector counts per 25 000 counts in monitor. Filled Gaussians represent fit results to the phonon peaks. Total fits are represented by full lines. Red color indicates results with a collimated beam, blue color represents data with the uncollimated beam.

disclose the uniqueness of the eigenstates and report an averaged $\hbar\omega = 11.4 \pm 0.2$ meV.

Energies of eigenstates identified at the Brillouin-zone boundary ($N$ point) are reported disclosed in Fig. 5. Γ- and $N$-point excitations up to 8 meV were utilized to renormalize the LDC results for a better match. Table I summarizes the experimental IN8@ILL, the pristine LDC, and the renormalized eigenfrequencies LDC*. Note that identical sequences of eigenstates at the points $x = 0.4$ and 0.5 ($N$ point) are observed in the experiment and calculated in both LDC and LDC* to be ta1, ta2, to1, la. Apart from the correspondence of the LDC and LDC* with IN8@ILL data this sequence emanates from the polarization dependent scans and is thus a unique argument for model discrimination of the $LaFe_4Sb_{12}$ lattice dynamics.

Figure 6 reports some spectra detected at different **Q** for the determination of the phonon dispersion along $[xxx]$. Unlike for the $[xx0]$ direction for which eigenmodes could be distinguished and followed over extended phase space regions of up to two Brillouin zones the eigenvectors for $[xxx]$ in the exploited scattering plane change notably resulting in a distinct intensity variation. For this reason a multiple of different symmetry-equivalent **Q** points were examined and distinction of the degenerate transverse and longitudinal modes were achieved by intensity discrimination. All identified energies are summarized in Fig. 7 and the $P$-point energy, which was exploited for LDC* is listed in Table I.

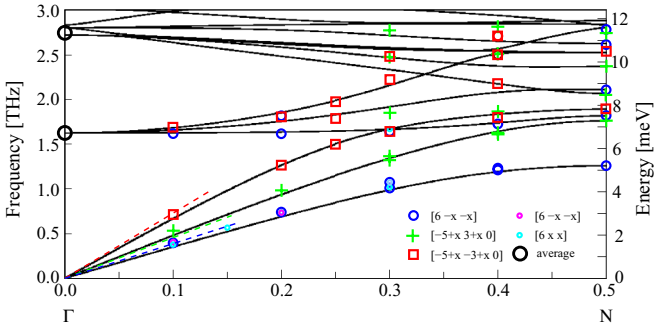


FIG. 5. (Color online) Phonon dispersion along $[xx0]$ derived from experiment (symbols) and determined by LDC* (solid lines). Reciprocal space points of the scans are reported in the figure. Scans $[6,-x,-x]$ are discriminated for the experimental setup with collimated beam (small circle) and ucollimated beam (large circle). Dashed lines represent elastic moduli data from Ref. [31].

Scans carried out at $(4-x,\ 4-x,\ 4-x)$ with $x = 0.2$, 0.25, and 0.3 were hampered by the physical limits of the spectrometer. The degenerate acoustic modes of transverse polarization could not be completely sampled towards low energies as can be judged from Fig. 6. Note that their energies derived from the fit of a single Gaussian miss accurate definition and deviate visibly towards lower energies in Fig. 7.

An equivalent approach as for the scans of $[xxx]$ phonons was applied to the determination of Brillouin-zone center (Γ-point) and zone boundary excitations. Some scans are reported in Fig. 8. Energies exploited for the renormalization of the LDC to LDC* are listed in Table I. The entire set of Γ-point scans indicates a number of maxima between 10 and 17 meV. Specific excitations can not be discerned accurately due to their high density. However, peaks around 11.5, 12.5, 14.5, and 16.5 meV are in agreement with the LDC* data as well as with calculations and Raman scattering results on $La_{0.75}Fe_3CoSb_{12}$ by Feldman *et al.* reported in Ref. [15].

### B. Force and elastic constants

We present in Table II the self-force constants $F^{n}_{ij}$ with n = La, Fe, and Sb obtained from the LDC* listed in Table I. Note that the $F^{n}_{ij}$ were effected by less than 1% by the performed

TABLE I. Energies of modes in meV at the Brillouin-zone center and zone boundary. LDC and LDC* characterize the results from the direct-method LDC based on the Hellmann-Feynman forces and taking into account the experimental IN8@ILL data, respectively. Unequivocally identified polarization of modes, such as transverse acoustic (ta), longitudinal acoustic (la), and transverse optic (to) are indicated with the monitored **Q**.

| | LDC | LDC* | IN8@ILL |
|---|---|---|---|
| Γ averaged | 6.91 | 6.72* | 6.72(1) |
| (6,−.5,−.5) ta1 | 5.35 | 5.21* | 5.21(1) |
| (−4.5,3.5,0) ta2 | 7.16 | 7.29* | 7.30(4) |
| (6,−.5,−.5) to1 | 7.72 | 7.52* | 7.52(4) |
| (−4.5,−2.5,0) la | 7.91 | 7.83* | 7.82(5) |
| *P* averaged | 7.27 | 7.18* | 7.17(5) |

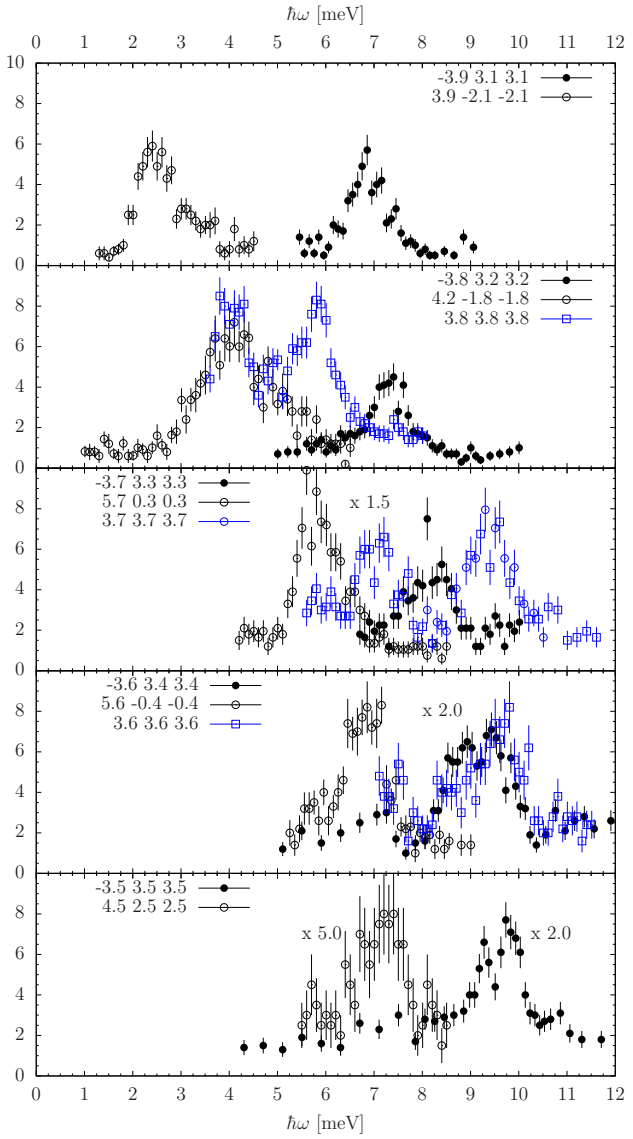


FIG. 6. (Color online) Phonon spectra measured along $[xxx]$. Intensity corresponds to detector counts per 25 000 counts in monitor. Some of the data sets have been scaled for clarity. The scaling factors are indicated in the subfigures.

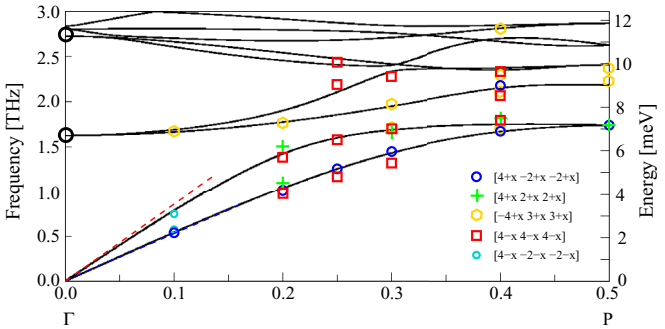


FIG. 7. (Color online) Phonon dispersion along $[xxx]$ derived from single-crystal INS data (symbols) and determined by LDC* (solid lines). Reciprocal space points of the scans are reported in the figure. Dashed lines represent elastic moduli which were computed according to experimental data from Ref. [31]

TABLE II. Self-force constants $F_{ij}^{n}$ ($n$ = La, Fe, Sb; $i, j = x, y, z$) in N/m from LDC*.

| | $xx$ | $yy$ | $zz$ | $xy$ | $xz$ | $yz$ |
|---|---|---|---|---|---|---|
| Fe | 174.8 | $xx$ | $xx$ | −12.3 | $xy$ | $xy$ |
| Sb | 161.0 | 98.6 | 101.1 | 0 | 0 | −2.1 |
| La | 51.1 | $xx$ | $xx$ | 0 | 0 | 0 |

frequency matching. Harmonic pair force constants are listed in Table III. Note that for presentation of the forces atomic positions have been chosen equivalent with the positions discussed by Feldman *et al.* in Ref. [20].

Table IV offers a comparison of elastic constants derived from the IN8@ILL experiment, from LDC* and estimated from ultrasonic pulse experiments reported in Ref. [31]. The elastic moduli were calculated as $C = \rho v^2$ with $\rho$ the mass density of completely filled $LaFe_4Sb_{12}$ with the lattice parameter $a = 9.135$ Å. The sound velocities $v$ were estimated from the acoustic phonon energies at $\mathbf{q} = (.1,.1,0)$ and $(.1,.1,.1)$ of IN8@ILL data, and at $(.01,.01,0)$, $(.01,.01,.01)$ and $(.01,0,0)$ of the LDC* results. Physical relations valid for moduli in different directions of a cubic crystal are indicated on top of Table IV.

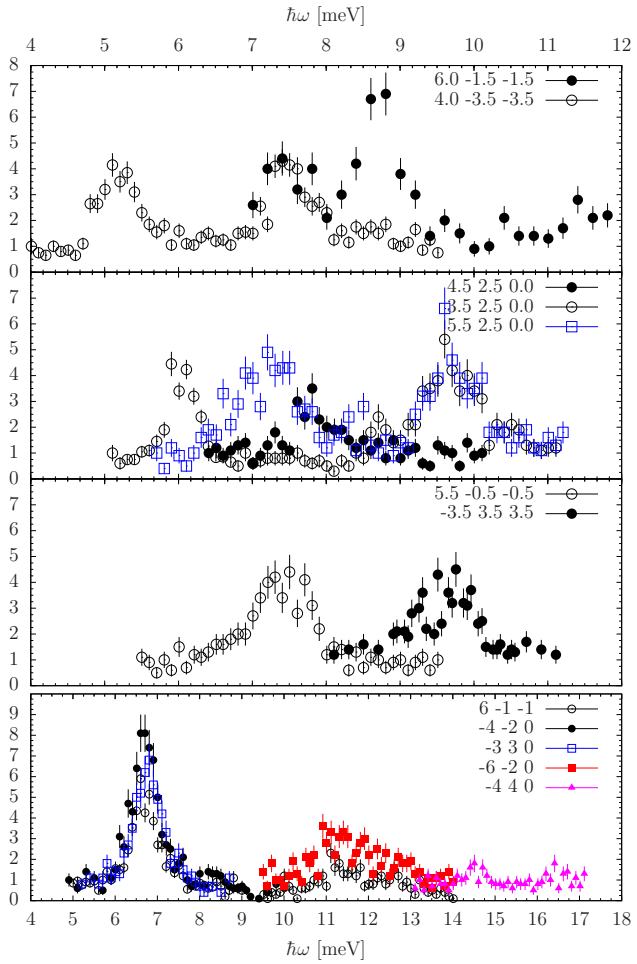


FIG. 8. (Color online) Excitations measured at the Brillouin-zone center and different zone boundary points. Intensity corresponds to detector counts per 25 000 counts in monitor.

TABLE III. Force constants $F_{ij}^{La-Sb}$ and $F_{ij}^{La-Fe}$ in N/m from LDC*. Fractional coordinates of considered atoms are La = (000), Sb1 = (−0.1635,0,0.3352), Sb2 = (−0.3365,1/2,0.1648), and Fe = (1/4,1/4,1/4).

| | La-Sb1 | La-Sb2 | La-Fe |
|---|---|---|---|
| $xx$ | −1.99 | 0.31 | 1.38 |
| $xy$ | 0 | 0.13 | 2.07 |
| $xz$ | 11.62 | 0.21 | 2.87 |
| $yx$ | 0 | −0.16 | 2.87 |
| $yy$ | 1.33 | −0.24 | 1.38 |
| $yz$ | 0 | 0.29 | 2.07 |
| $zx$ | 9.37 | −0.40 | 2.07 |
| $zy$ | 0 | 0.01 | 2.87 |
| $zz$ | –15.31 | −0.18 | 1.38 |

They were exploited to compute $C_{11}$ from IN8@ILL and $C_{11}$, $C^{iii}$, and $C^{iv}$ from Ref. [31]. We discriminated the elastic constants along $\mathbf{q}$||[x00] whose degeneracy is lifted due to the octahedra distortion in skutterudites as $C'_{44}$ and $C''_{44}$ [2,32,33].

We estimated the bulk moduli through $B = C_{11} - 2C^{iii} + 2/3C_{44}$ to be 98(8) GPa (IN8@ILL), 85 GPa (LDC*), and 98 GPa (Ref. [31]).

### C. Phonon intensities

Figure 9 reports phonon intensities calculated and measured along $\mathbf{q}$||[xx0]. The area of the full circles represent the LDC* intensity whereas measured intensities are represented by the area of the empty circles. All intensities are scaled in respect to the signal of the [3Tu(I)] Γ-point excitation indicated at $x = 1.0$ in Fig. 9. This intensity was determined experimentally at $(6, -1, -1)$. Intensities derived at symmetry-equivalent points were scattering within ±5% of the $(6, -1, -1)$ intensity. To compare LDC* and experimental results all measured data were corrected for the thermal occupation by the

TABLE IV. Elastic constants in GPa derived from the experiment at IN8@ILL, computed through LDC*, and from literature data of Ref. [31]. The elastic constants are characterized by the polarization of the corresponding acoustic phonons as transverse acoustic mode of lower (ta1) and higher (ta2) energy, and longitudinal acoustic phonon (la).

| | $\mathbf{q}$\|\|[x00] | $\mathbf{q}$\|\|[xx0] | $\mathbf{q}$\|\|[xxx] |
|---|---|---|---|
| ta1 | $C'_{44}$ | $C_{44}$ | $C^{iii} = \frac{2C^{i}+C_{44}}{3}$ |
| ta2 | $C''_{44}$ | $C^{i} = \frac{C_{11}-C_{12}}{2}$ | $C^{iii}$ |
| la | $C_{11}$ | $C^{ii} = \frac{C_{11}+C_{12}+2C_{44}}{2}$ | $C^{iv} = \frac{4C^{ii}-C_{11}}{3}$ |
| IN8@ILL | – | 49(1)† | 60(1)† |
| | – | 94(2) | 60(1)† |
| | 186(10)[a] | 169(2)† | 122(5) |
| LDC* | 40 | 41 | 66 |
| | 43 | 80 | 66 |
| | 190 | 153 | 141.0 |
| Ref. [31] | – | 49.4‡ | 61.9[b] |
| | – | 68.2‡ | 61.9[b] |
| | 189.1/194.5[b] | 175.7‡ | 163.9[b] |

[a]Computed from values marked with †.
[b]Computed from values marked with ‡.

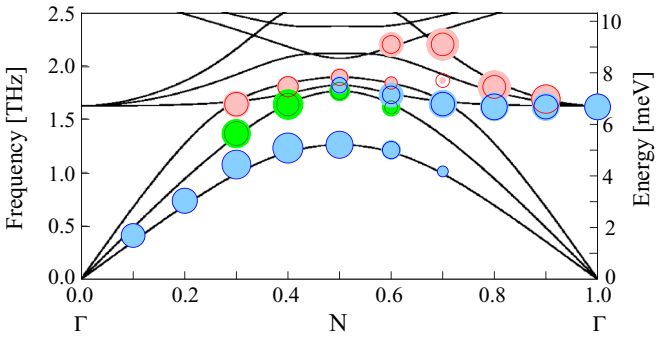


FIG. 9. (Color online) Phonon intensities sketched on the phonon dispersion lines. Intensities are indicated by the area of the circles and scaled to the intensity at Γ point $x = 1.0$. Full and empty circles represent the LDC* and measured intensities, respectively.

Bose-Einstein factor $n(\omega,T)$ and for an average count rate in monitor 2.

It is necessary and worth commenting that the depicted intensities were selected for the distinctness of the probed eigenmodes. For spectra with overlapping peaks, weak signals, and high background levels the applied match by a number of Gaussians and a flat constant background did not result in fit parameters of peak intensities and peak widths for an interpretation on solid quantitative grounds. These were in general spectra probing the $[xxx]$ dispersion and Γ-point modes beyond the first optic 3Tu(I) excitation. Nonetheless the qualitative variation of the peak intensities within the scans was correctly predicted by the LDC*.

Another point deemed necessary commenting are the experimental intensities of the ta1 mode indicated at $x = 0.1$ and 0.2 in Fig. 9. They were derived from data with uncollimated beam and thus prone to depict signal from modes of distinct polarization.

The general correspondence between the measured and calculated results is reasonably good for the distinguished modes along $[xx0]$ and at high-symmetry points. A weak, however notable, underestimation of the intensity of localized modes in respect to the reference and to the ta1 mode intensities is observable.

## IV. CONCLUSIONS AND OUTLOOK

It has been shown that first-principles-based lattice dynamics calculations reproduce the vibrational dynamics of the $LaFe_4Sb_{12}$ compound in the energy range of high lanthanum amplitudes accurately. Both, the measured phonon dispersion $\hbar\omega(\mathbf{Q})$ determined by the dynamical matrix and, thus, by the atomic potentials as well as the phonon intensities determined by the phonon eigenvectors are matched to a high degree [34–36]. Unlike the computer-generated structure the experimentally studied specimen was tested to be a lanthanum-deficient compound with the stoichiometry $La_{0.90\pm0.04}Fe_4Sb_{12}$. The effect of such deficiency on the phonon dispersion and eigenvectors can not be judged upon reliably without further computer studies. It should have, however, an immediate consequence through the reduced scattering power of La on the recorded intensity. We expect this effect to be stronger established in the range of energies with high La contribution, i.e., on the localized low-energy modes. In line with this basic explanation a diminished intensity of localized modes has been observed on a relative scale.

At the high-symmetry point $N$ the experimental as well as the LDC* data have established a characteristic sequence of eigenmodes. Thereby, the transverse optic mode of lowest energy crosses the longitudinal acoustic phonon around $x = 0.3$. Within the present computation approach this solution is robust as it is as well a solution of the pristine LDC calculation, i.e., derived without taking experimental data into account, and a $1 \times 1 \times 1$ super cell resulted in equivalent eigenmode sequence at point $N$. This result deserves some attention as it can serve as a unique argument for the discrimination of the applicability of distinct DFT approximations and LDC models. Rotter *et al.* successfully applied this approach in Ref. [17] to the vibrational dynamics of $Co_4Sb_{12}$ probed by inelastic x-ray scattering. They compared eigenfrequencies and eigenvectors obtained from different DFT approximations and LDC models at the high-symmetry point $H$ (.5,0,0) and identified this way a model approximating best the experimental data.

Feldman *et al.* have presented in Ref. [9] the phonon dispersion of $LaFe_4Sb_{12}$ calculated on the grounds of DFT within the LDA. In general, the phonon properties in Ref. [9] match well with the here established eigenmode scheme. We point out only the symmetry-avoided anticrossing of eigenmodes in both directions $\Gamma \rightarrow N$ and $\Gamma \rightarrow P$ whose correctness is confirmed unequivocally in this work by experiment. However, an obvious difference between the present data and the results of Feldman *et al.* is the different sequence of eigenmodes at point $N$, where in the later case the optic mode is located between the two acoustic modes of transverse polarization and, thus, crosses two acoustic modes, namely the longitudinal and the higher-energy transverse acoustic modes. It is an interesting, however open, question whether calculations on an expanded supercell as recently published by Feldman *et al.* in Ref. [20] could have lifted this difference.

The computed self-force constant of lanthanum takes on a value about 10–15 % higher than the constants derived through different approximations and models by Feldman *et al.* in Refs. [15] and [20]. The La-La (0,0,0)-(1/2,1/2,1/2) harmonic force constant ($F_{xx}^{\mathrm{La,La}} = F_{yy}^{\mathrm{La,La}} = F_{zz}^{\mathrm{La,La}} = 0.11$ N/m) exceeds the results from the different approaches in Ref. [20] by a factor of 5 up to 2 orders of magnitude. Harmonic force constants calculated here match the scatter of data within the different model results of Feldman *et al.* Overall, they indicate that the force exerted on La is slightly higher in the present computer model with a particularly enhanced interaction between the La sites. In a simplified picture we may expect from a stronger coupling a higher dispersivity of the La-weighted eigenmodes.

For cubic symmetry the elastic constants fulfill a set of strict relations [37]. These relations are met by the results reported in Ref. [31] and the present LDC* data. The values computed from the TAS data do not fully satisfy conditions (iv) and (v) of Ref. [37]. Although at the lowest $\mathbf{q}$ numbers sampled in the experiment the dispersion of the acoustic modes departs already from the linear relation of acoustic phonons at $\mathbf{q} \rightarrow \mathbf{0}$, as firmed up by our LDC* data, we account $C^i$ and $C^{iv}$ for the observed discrepancy. Both differ markedly from the elastic constants sampled in the long-wavelength limit in Ref. [31]

and by the LDC*. The bulk modulus calculated from $C_{44}$, $C^{ii}$, and $C^{iii}$ corresponds well with the long-wavelength limit literature data and approximates the result of $B = 88.7$ GPa obtained on polycrystalline $LaFe_4Sb_{12}$ material [38].

We expect the disorder due to the La-deficiency as well as the finite temperature to reduce the phonon lifetimes and, thus, to increase the phonon widths. However, within the accuracy of the experimental data the derived phonon widths were approximated satisfactorily by the performed RESTRAX calculations, i.e., by the expected instrument resolution. On purely experimental grounds, for scans at lowest **q** performed with the collimated beam, the Gaussian widths of the probed elastic peaks and of the inelastic signal match as indicated in Fig. 5. As a consequence, with the applied experimental setup the effect of temperature might become detectable only as a renormalization of phonon frequencies. To trace changes in the phonon lifetime techniques are required with energy resolutions improved by at least one order of magnitude, such as a neutron spin-echo TAS instrument. Experiments are a subject for future studies.

## ACKNOWLEDGMENTS

We would like to thank Juri Grin for his steady interest and encouragement. We appreciate the invaluable long-time support from YuG 23–07–1955. The authors thank Ulrich Burkhardt for the microprobe analysis, and Jacques Ollivier and Bachir Ouladdiaf for the access to the instruments IN5@ILL and OrientExpress@ILL.

[1] I. Oftedal, Z. Kristallogr. **66**, 517 (1928).
[2] A. Kjekshus and T. Rakke, Acta Chem. Scand. A **28**, 99 (1974).
[3] B. C. Sales, B. Mandrus, and R. K. Williams, Science **272**, 1325 (1996).
[4] G. P. Meisner, D. T. Morelli, S. Hu, J. Yang, and C. Uher, Phys. Rev. Lett. **80**, 3551 (1998).
[5] P. F. Qiu, J. Yang, R. H. Liu, X. Shi, X. Y. Huang, G. J. Snyder, W. Zhang, and L. D. Chen, J. Appl. Phys. **109**, 063713 (2011).
[6] N. Bernstein, J. L. Feldman, and D. J. Singh, Phys. Rev. B **81**, 134301 (2010).
[7] H. Geng, X. Meng, H. Zhang, and J. Zhang, J. Appl. Phys. **116**, 163503 (2014).
[8] V. Keppens, D. Mandrus, B. C. Sales, B. C. Chakoumakos, P. Dai, R. Coldea, M. B. Maple, D. A. Gajewski, E. J. Freeman, and S. Bennington, Nature (London) **395**, 876 (1998).
[9] J. L. Feldman, P. Dai, T. Enck, B. C. Sales, D. Mandrus, and D. J. Singh, Phys. Rev. B **73**, 014306 (2006).
[10] R. Viennois, L. Girard, D. Ravot, H. Mutka, M. Koza, F. Terki, S. Charar, and J.-C. Tedenac, Physica B **350**, E403 (2004).
[11] R. Viennois, L. Girard, M. M. Koza, H. Mutka, D. Ravot, F. Terki, S. Charar, and J.-C. Tedenac, Phys. Chem. Chem. Phys. **7**, 1617 (2005).
[12] M. M. Koza, M. R. Johnson, R. Viennois, H. Mutka, L. Girard, and D. Ravot, Nature Mater. **7**, 805 (2008).
[13] H. D. Lutz and G. Kliche, Physica Status Solidi B **112**, 549 (1982).
[14] G. Kliche and H. Lutz, Infrared Phys. **24**, 171 (1984).
[15] J. L. Feldman, D. J. Singh, C. Kendziora, D. Mandrus, and B. C. Sales, Phys. Rev. B **68**, 094301 (2003).
[16] L. Li, H. Liu, J. Wang, X. Hu, S. Zhao, H. Jiang, Q. Huang, H. Wang, and Z. Li, Chem. Phys. Lett. **347**, 373 (2001).
[17] M. Rotter, P. Rogl, A. Grytsiv, W. Wolf, M. Krisch, and A. Mirone, Phys. Rev. B **77**, 144301 (2008).
[18] J. L. Feldman, D. J. Singh, I. I. Mazin, D. Mandrus, and B. C. Sales, Phys. Rev. B **61**, R9209 (2000).
[19] R. Viennois, S. Charar, D. Ravot, P. Haen, A. Manger, A. Bentien, S. Paschen, and F. Steglich, Eur. Phys. J. B **46**, 257 (2005).
[20] J. L. Feldman, D. J. Singh, and N. Bernstein, Phys. Rev. B **89**, 224304 (2014).
[21] S. Tsutsui, H. Uchiyama, J. P. Sutter, A. Q. R. Baron, M. Mizumaki, N. Kawamura, T. Uruga, H. Sugawara, J.-i. Yamaura, A. Ochiai *et al.*, Phys. Rev. B **86**, 195115 (2012).
[22] S. Tsutsui, H. Kobayashi, J. P. Sutter, H. Ushiyama, A. Q. R. Baron, Y. Yoda, D. Kikuchi, H. Sugawara, C. Sekine, I. Shirotani *et al.*, J. Phys. Soc. Jpn. **77**, 257 (2008), suppl. A.
[23] J. Yang, W. Zhang, S. Q. Bai, Z. Mei, and L. D. Chen, Appl. Phys. Lett. **90**, 192111 (2007).
[24] C. Lee, I. Hase, H. Sugawara, H. Yoshizawa, and H. Sato, J. Phys. Soc. Jpn. **75**, 123602 (2006).
[25] J. Saroun and J. Kulda, *Modern Developments in X-Ray and Neutron Optics* (Springer, Berlin, 2008), pp. 57–68.
[26] K. Parlinski, in *Neutrons and Numerical Methods N2M*, edited by M. R. Johnson, G. J. Kearley, and H.G. Büttner, AIP Conf. Proc. No. 479 (AIP, New York, 1999), pp. 121–126.
[27] K. Parlinski, Z. Q. Li, and Y. Kawazoe, Phys. Rev. Lett. **78**, 4063 (1997).
[28] G. Kresse and J. Furthmueller, Comput. Mater. Sci. **6**, 15 (1996).
[29] G. Kresse and D. Joubert, Phys. Rev. B **59**, 1758 (1999).
[30] M. Marek Koza, D. Adroja, N. Takeda, Z. Henkie, and T. Cichorek, J. Phys. Soc. Jpn. **82**, 114607 (2013).
[31] I. Ishii, T. Fujita, I. Mori, H. Sugawara, M. Yoshizawa, K. Takegahara, and T. Suzuki, J. Phys. Soc. Jpn. **78**, 084601 (2009).
[32] A. Kjekshus, D. G. Nicholson, and T. Rakke, Acta Chem. Scand. **27**, 1307 (1973).
[33] D. J. Braun and W. Jeitschko, J. Less Common Metals **72**, 147 (1980).
[34] N. Ashcroft and N. Mermin, *Solid State Physics* (Saunders College, Philadelphia, 1976).
[35] G. Squires, *Introduction to the Theory of Thermal Neutron Scattering* (Dover Publications, Mineola, 1996).
[36] A. A. Maradudin, E. W. Montroll, G. H. Weiss, and I. P. Ipatova, *Theory of Lattice Dynamics in the Harmonic Approximation* (Academic Press, Waltham, 1971).
[37] The elastic constants probed along **q**||[xx0] and **q**||[xxx] are related as (i) $C_{11} = C^i + C^{ii} - C_{44}$, (ii) $C_{11} = C^{ii} + 3/2C^{iii} - 3/2C_{44}$, (iii) $C_{11} = 4/3C^i + C^{iv} - 4/3C_{44}$, (iv) $C_{11} = 4C^{ii} - 3C^{iv}$, (v) $0 = 2C^i + C_{44} - 3C^{iii}$.
[38] C. Recknagel, N. Reinfried, P. Höhn, W. Schnelle, H. Rosner, Y. Grin, and A. Leithe-Jasper, Sci. Technol. Adv. Mater. **8**, 357 (2007).